CHAPTER 1

Overview of Low Frequency data

1.1 Introduction . At long periods, it is convenient (and quite accurate) to think of a seismogram simply as a sum of decaying cosinusoids :

$$u(t) = \sum_{k=1}^{\infty} A_k \cos(\omega_k t + \phi_k) e^{-\alpha_k t} \tag{1.1}$$

where $u(t)$ is the observed time series, A_k and ϕ_k are the initial amplitude and phase of the k'th mode of oscillation, and ω_k and α_k are the frequency and attenuation rate. The usual analogy that is made is that of a bell. When we hit a bell, the resulting sound consists of certain discreet frequencies - the tones of the bell. These frequencies and the rate at which the oscillations decay are properties of the structure of the bell. The actual sound we produce depends upon how we hit the bell. Obviously, the harder we hit the bell, the larger the initial amplitude of the oscillations. Depending upon where and how we hit the bell, we can excite some oscillations more than others. In terms of 1.1, ω_k and α_k tell us about Earth structure and A_k and ϕ_k tell us about the Earthquake source.

The attenuation rate is sometimes specified by the "quality factor" of the oscillation, Q_k,where

$$\alpha_k = \omega_k / 2Q_k. \tag{1.2}$$

If Q_k is large, α_k is small and the oscillation rings on for a long time. Conversely, an oscillation with a small Q_k is rapidly damped out. The low frequency oscillations which we are considering (*i.e.*, frequency less than $10mHz$) have Q_k between about 100 and 6000. Thus $\alpha_k \ll \omega_k$ and attenuation is weak.

A seismogram is the interference pattern of a sum of many decaying sinusoids (Fig 1.1). To see the individual modes of oscillation we work in the frequency domain by Fourier transforming. Our definition of the forward Fourier transform (*i.e.*, time to frequency) is

$$f(\omega) = \int_{-\infty}^{\infty} f(t) e^{-i\omega t} dt. \tag{1.3}$$

$f(\omega)$ is a complex quantity called the "spectrum" of $f(t)$.
We are interested in the spectrum of a decaying cosinusoid. Let

$$\begin{aligned} C_k(t) &= \cos(\omega_k t) e^{-\alpha_k t} \qquad \text{for} \quad t \geq 0, \\ C_k(t) &= 0 \qquad \text{for} \quad t < 0. \end{aligned}$$

then

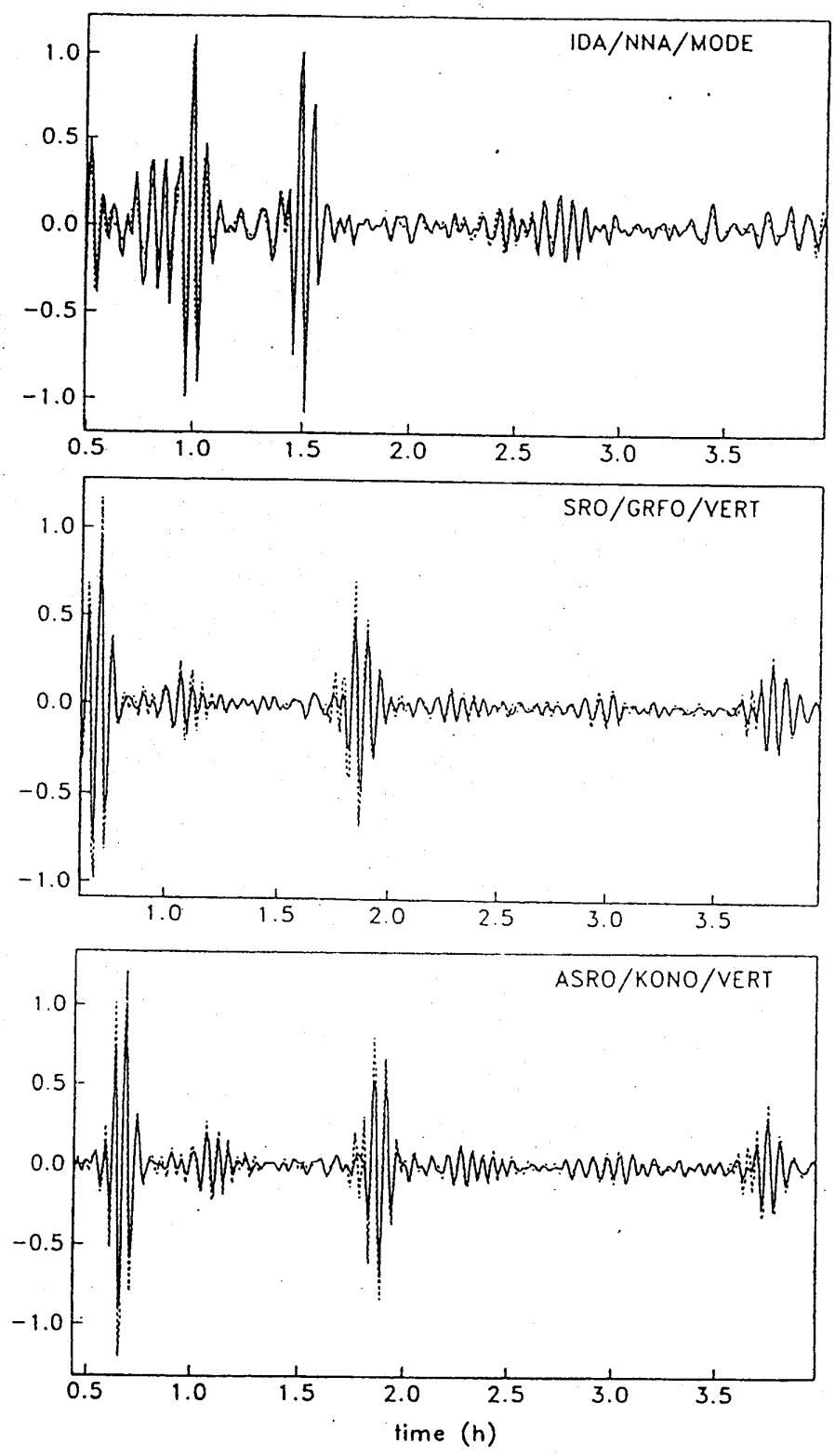

Figure 1a. A comparison of long period waveforms (T > 150 secs) with spherical Earth synthetic seismograms for a large deep (450km) event (Banda Sea 1982/173). Note that fundamental mode Rayleigh wave packets dominate even the recordings of very deep events at these periods.

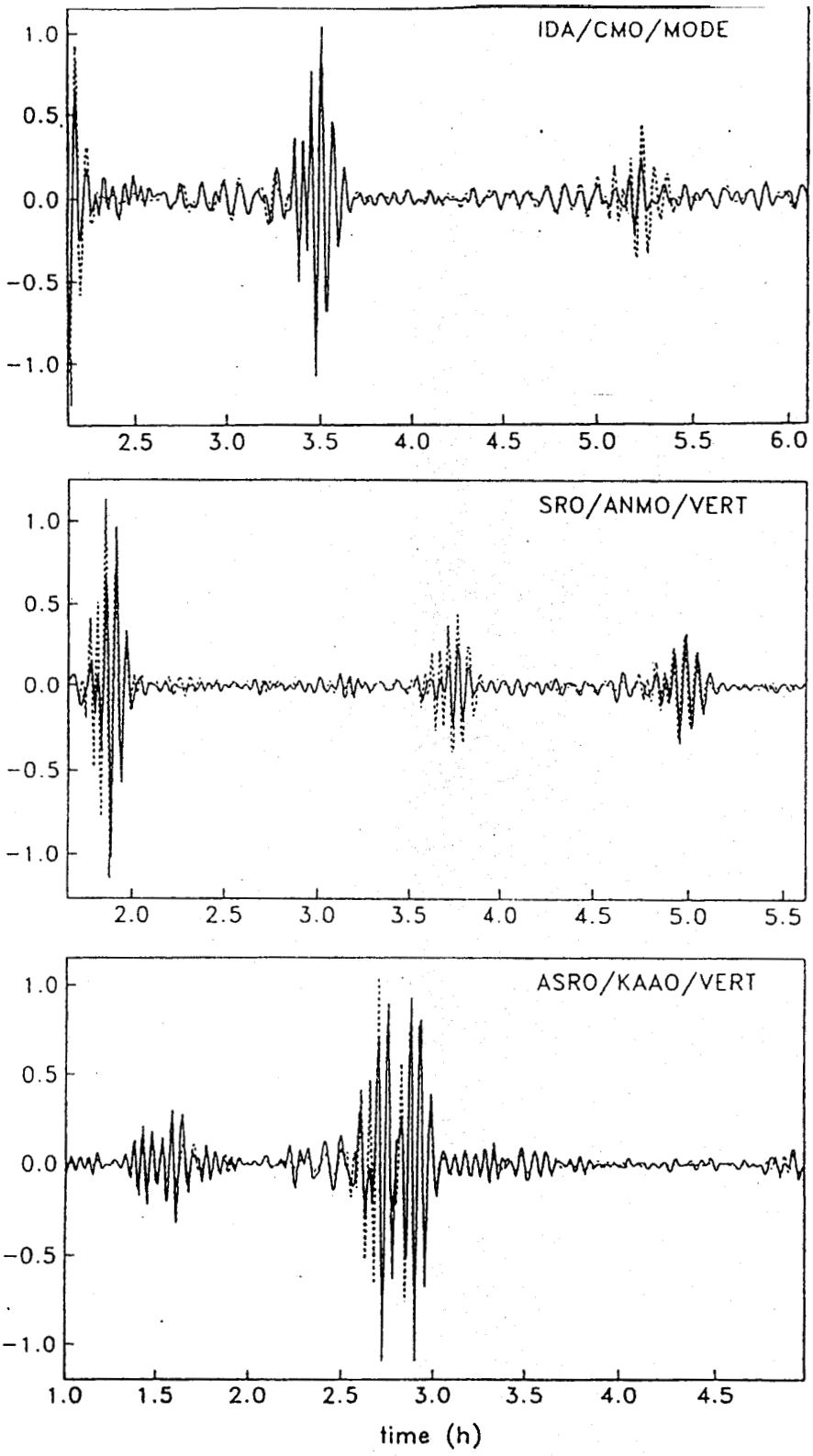

Figure 1b. As for fig1a except for a large shallow event (Iran 1978/259).

$$
\begin{aligned}
C_k(\omega) &= \int_0^\infty \cos(\omega_k t) e^{-\alpha_k t} e^{-i\omega t} dt, \\
&= \tfrac{1}{2} \int_0^\infty (e^{(-\alpha_k + i(\omega_k - \omega))t} + e^{(-\alpha_k - i(\omega_k + \omega))t}) dt, \\
&= \tfrac{1}{2} \frac{1}{\alpha_k - i(\omega_k - \omega)} + \tfrac{1}{2} \frac{1}{\alpha_k + i(\omega_k + \omega)}.
\end{aligned}
$$

For $\omega \simeq \omega_k$, the first term is large whilst the second term is much smaller. Thus, if we only consider positive frequencies in the vicinity of ω_k, we have

$$
C_k(\omega) \simeq \tfrac{1}{2} \frac{1}{\alpha_k - i(\omega_k - \omega)} \tag{1.4}
$$

or, in terms of real and imaginary parts,

$$
C_k(\omega) = \tfrac{1}{2} \frac{\alpha_k}{\alpha_k^2 + (\omega_k - \omega)^2} + i \tfrac{1}{2} \frac{(\omega_k - \omega)}{\alpha_k^2 + (\omega_k - \omega)^2} \tag{1.5}
$$

$C_k(\omega)$ is plotted in Fig. 1.2. Note that the real part falls off from its peak value as $(\omega_k - \omega)^2$ whereas the imaginary part falls off only as $(\omega_k - \omega)$. This latter property means that the spectrum of a decaying sinusoid falls off quite slowly from its peak value ($\approx 6db/octave$).

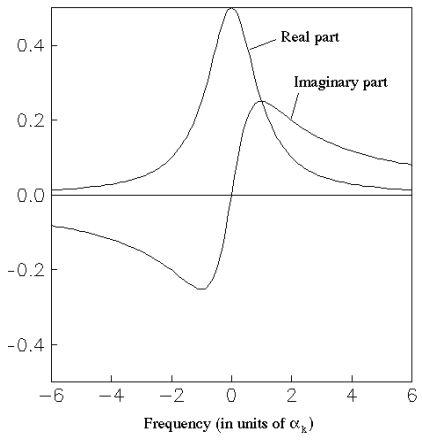

Fig 1.2 Spectrum of a decaying cosinusoid in a small frequency band surrounding the center frequency, ω_k. Frequency is in units of α_k

Problem 1.1 Show that the width of the power spectrum of $C_k(\omega)$ at the half power points is $2\alpha_k$.

The seismogram is a sum of such spectra all centered at different frequencies so a plot of the modulus

of the spectrum of 1.1 looks something like the following sketch:

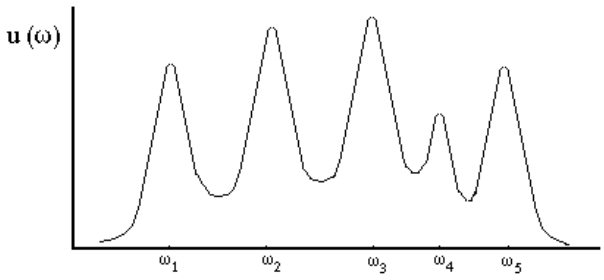

You should note a couple of things. First, each spectral peak falls off quite slowly so modes of oscillation which are close together in frequency may not be resolvable as separate peaks. Second, the width of a spectral peak is related to α_k (actually, the width of a peak at the half-power points is $2\alpha_k$). Thus, weakly attenuated modes have narrow spectral peaks while strongly attenuated modes have broad peaks.

An application of this procedure to a real time series is shown in Fig 1.3. The only difference between this result and our previous analysis is that, for obvious reasons, we did not use an infinite record length. Peaks are clearly visible but their long tails overlap and the result is quite messy. The result can be improved by using a *data window* (or *taper*). The procedure is to multiply the finite data series by some chosen function of time before Fourier transforming. The very act of taking a finite record length is equivalent to multiplying an infinite record by a boxcar function but such a function has very poor *spectral leakage* characteristics. To illustrate what this means, consider the result of multiplying the time series by a Hanning taper (which is illustrated in Fig 1.5) before Fourier transforming. The result, shown in Fig 1.4, is much less jagged than before and the peaks are more clearly defined. The simplest way to understand this result is in terms of *convolution*. Convolution is discussed in all text books on time series analysis and so will only be given brief consideration here.

The convolution of two functions of time, $a(t)$ and $b(t)$, is defined by:

$$a(t) * b(t) = \int_{-\infty}^{\infty} a(t - t')b(t')\, dt'. \tag{1.6}$$

Then

$$F.T.(a * b) = a(\omega) \cdot b(\omega)$$

$$F.T.(a \cdot b) = a(\omega) * b(\omega)$$

where $F.T.$ stands for "Fourier transform of"

Taking a finite record length of data is equivalent to multiplying the infinite record by a boxcar, $B(t)$

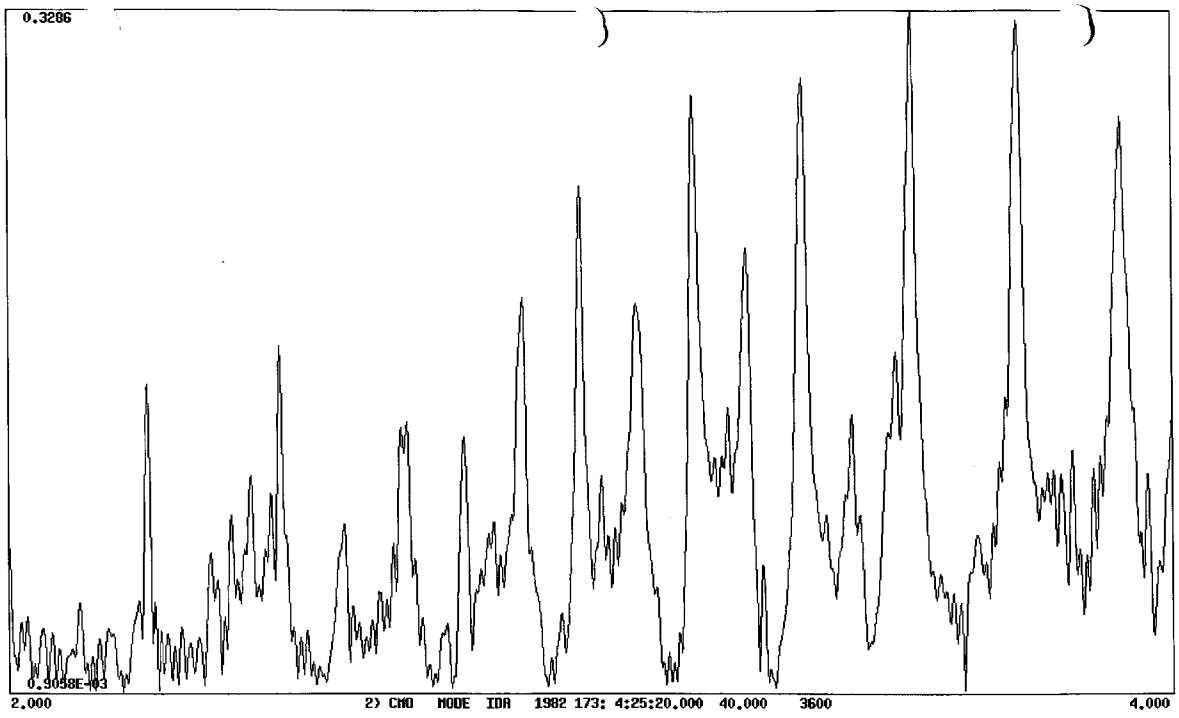

Figure 1.3. A spectrum between 2 and 4 mHz with no taper applied.

of length T:

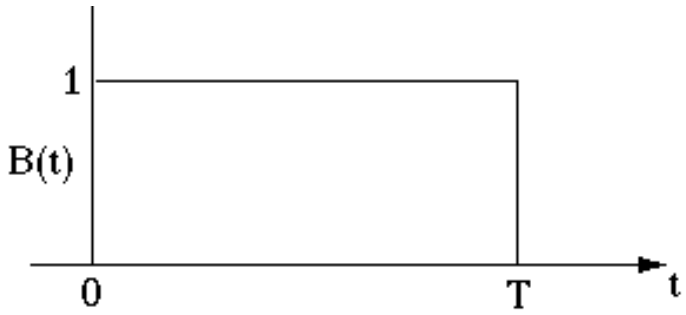

In the frequency domain, this is equivalent to convolving $u(\omega)$ with $B(\omega)$. Now

$$B(\omega) = \int_{-\infty}^{\infty} B(t)e^{-i\omega t}dt = \int_{0}^{T} e^{-i\omega t}dt = \frac{e^{-i\omega T}-1}{-i\omega} = Te^{i\omega T/2}\frac{\sin(\omega T/2)}{(\omega T/2)}$$

The spectrum $B(\omega)$ is a phase shift multiplied by a sinc function. If we sketch the modulus of this

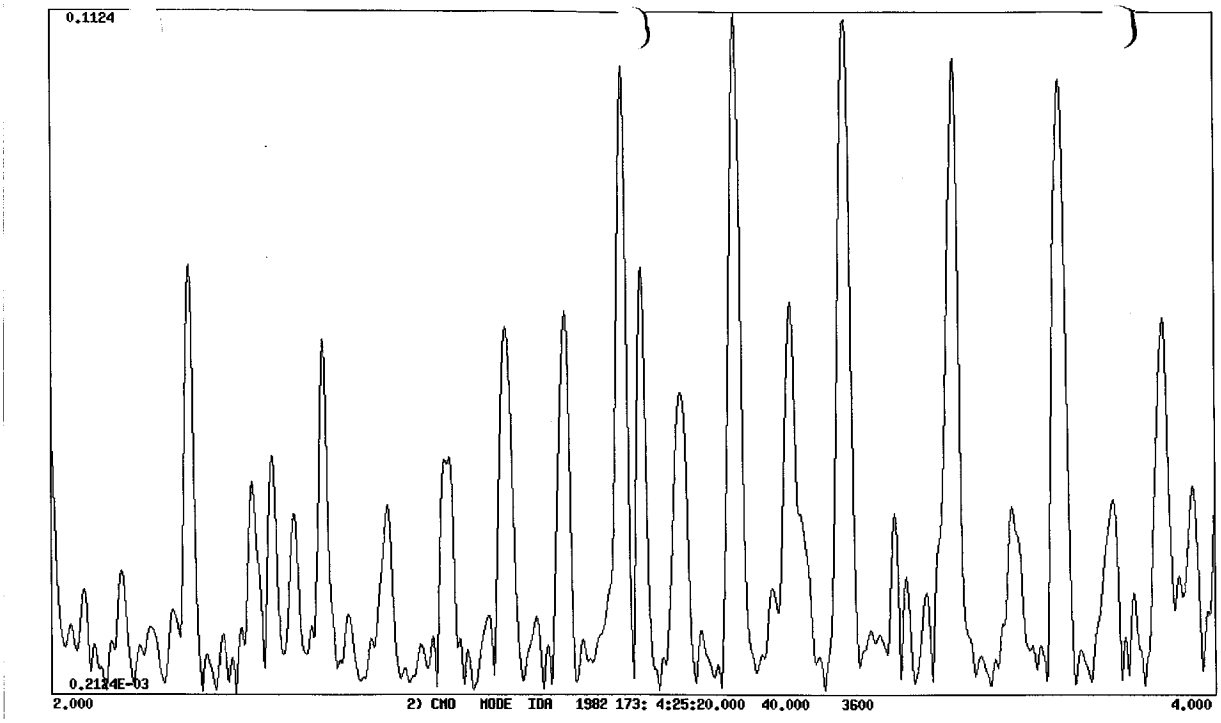

Figure 1.4. The same spectrum as fig 1.3 but with a Hanning taper applied.

function it looks like

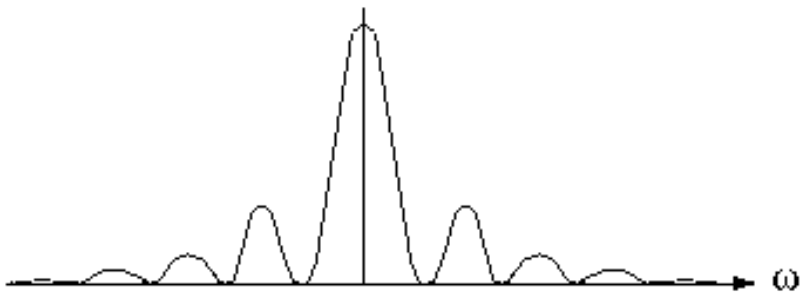

Convolution with a peak-like function (*i.e.*, the spectrum of a decaying sinusoid) gives a spectrum very

much like that of a boxcar, *i.e.*,

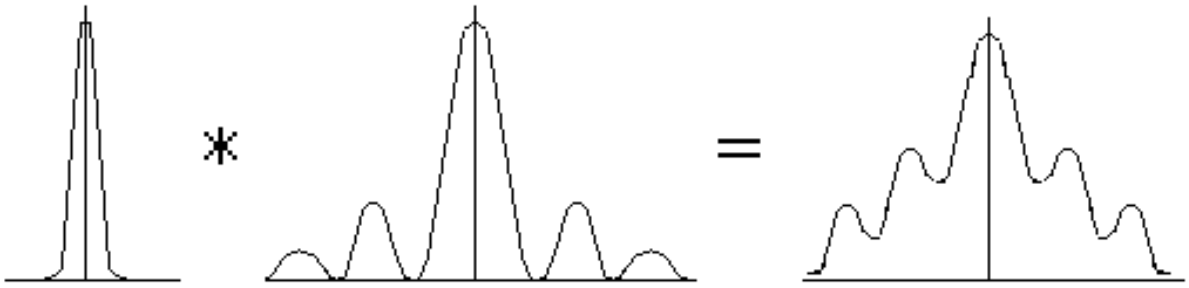

Thus, with a finite record length, we do not see the spectrum of a resonance function, but we see a function with sidelobes. Energy originally at a frequency ω_k now appears at other frequencies, *i.e.*, the frequencies of the sidelobes. This phenomenon is called *spectral leakage* and is responsible for the jagged appearance of the spectrum in Figure 1.3 (and is partially responsible for the appearance of energy between the peaks corresponding to the free oscillation frequencies).

If we do not use a data window, we are implicitly using a boxcar function but obviously we can choose any function we like. The choice of an optimal window is quite complicated as there are trade-offs involved. In particular, we would like to choose a data window with a spectrum which has very small sidelobes to reduce spectral leakage. At the same time, we would like the central lobe of the spectrum of the data window to be narrow so that we have as much frequency resolution as possible. The log-modulus of the spectrum of several data windows are shown in Figure 1.5. (The log helps to emphasize the size of the sidelobes.) A cosine data window suppresses the sidelobe level but broadens the central lobe. A $\cos^2$ data window suppresses sidelobes even more but the central peak is further broadened. Other tapers can be devised which essentially have no sidelobes but are too broad for our application. Harris, (1978) reviews many of the tapers in common usage. Some work has been done on finding optimal tapers for a time series of decaying cosinusoids and a general (but difficult) review of spectrum estimation and harmonic analysis is by Thomson (1982). Figure 1.6 shows spectra of a time series using some of these windows. These tapers are quite difficult to compute and we content ourselves here with choosing a compromise data window such as the Hanning window.

The desirability of using a data window is illustrated in Figure 1.7 by a synthetic example (Dahlen 1982). The top panel illustrates the spectrum of a time series consisting of ten modes of oscillation with frequencies indicated by the vertical lines. If we were simply to estimate the mode frequencies by picking peaks, it is clear that we would get significantly biased estimates. The application of the Hanning window ($\cos^2$) gives the result in the middle panel. The peaks are now separated and centered at their true frequencies. Another window (Blackman-Harris 4-term, BHV) has been applied in the lower panel. The spectral leakage is much less than for the Hanning taper but the peak widths are broader and two closely spaced lines would not be as well resolved as with the Hanning taper. The Hanning taper is therefore a reasonable compromise.

The application of a data window has two desirable effects. It reduces spectral leakage and it modifies the shape of the spectrum of a decaying cosinusoid making it more concentrated in frequency. This latter property means that individual peaks in the spectrum can be more clearly identified (though peak widths are now no longer simply related to α_k).

1.2 Estimation of peak frequencies. **.** To learn about Earth structure, we would like to measure ω_k and α_k and similarly, to learn about the earthquake source, we would like to measure A_k and ϕ_k. An obvious way to measure ω_k is to just take the peak value of the spectrum. This is not a very good procedure as the peak value can be biased when modes are closely spaced in frequency. Furthermore,

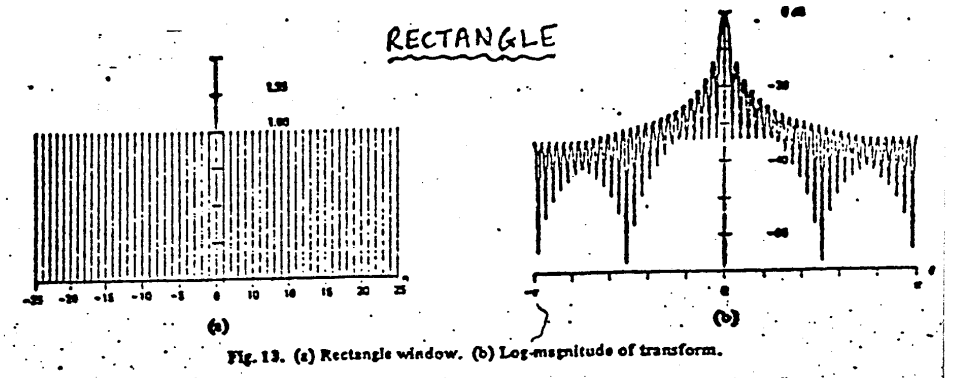

Fig. 13. (a) Rectangle window. (b) Log-magnitude of transform.

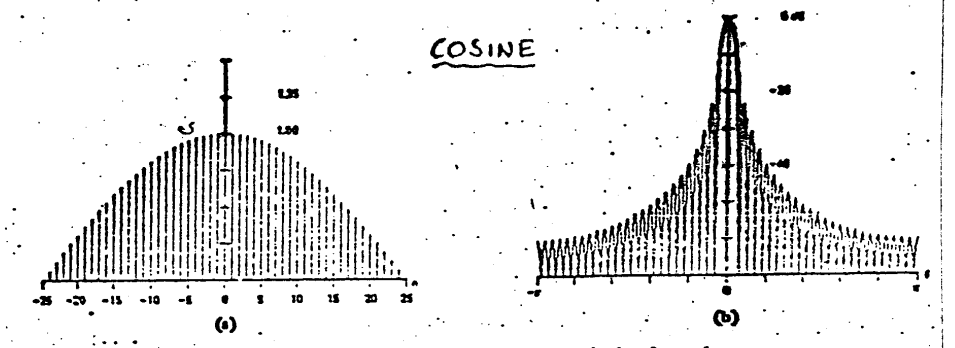

Fig. 16. (a) Cos ($n\pi/N$) window. (b) Log-magnitude of transform.

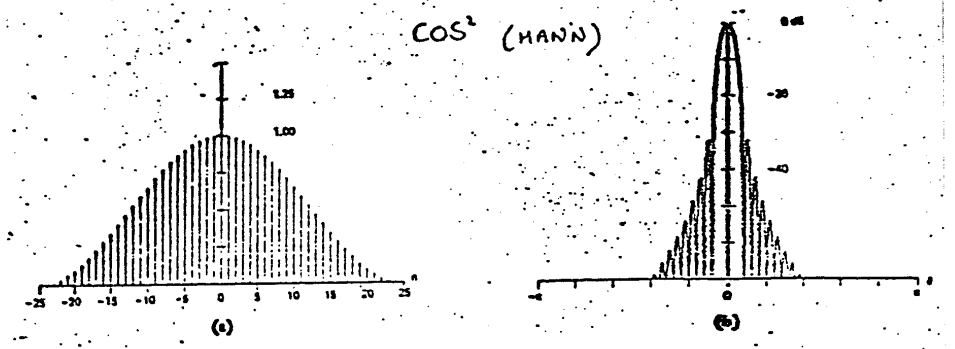

Fig. 17. (a) Cos² ($n\pi/N$) window. (b) Log-magnitude of transform.

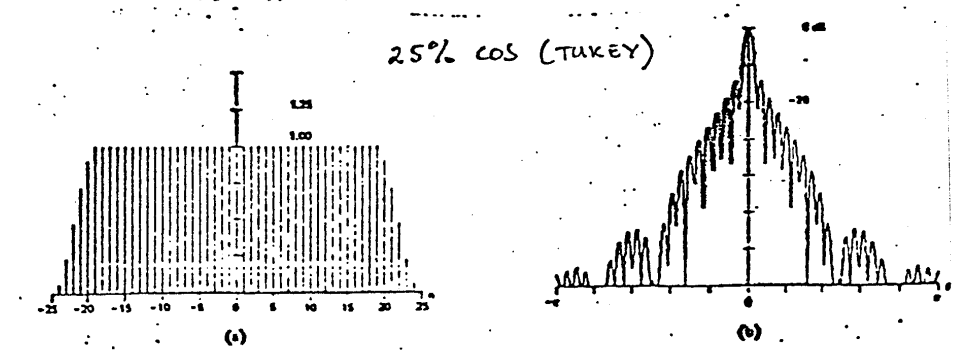

Fig. 30. (a) 25-percent cosine taper (Tukey) window. (b) Log-magnitude of transform.

Figure 1.5. Various tapers and their log amplitude spectra.

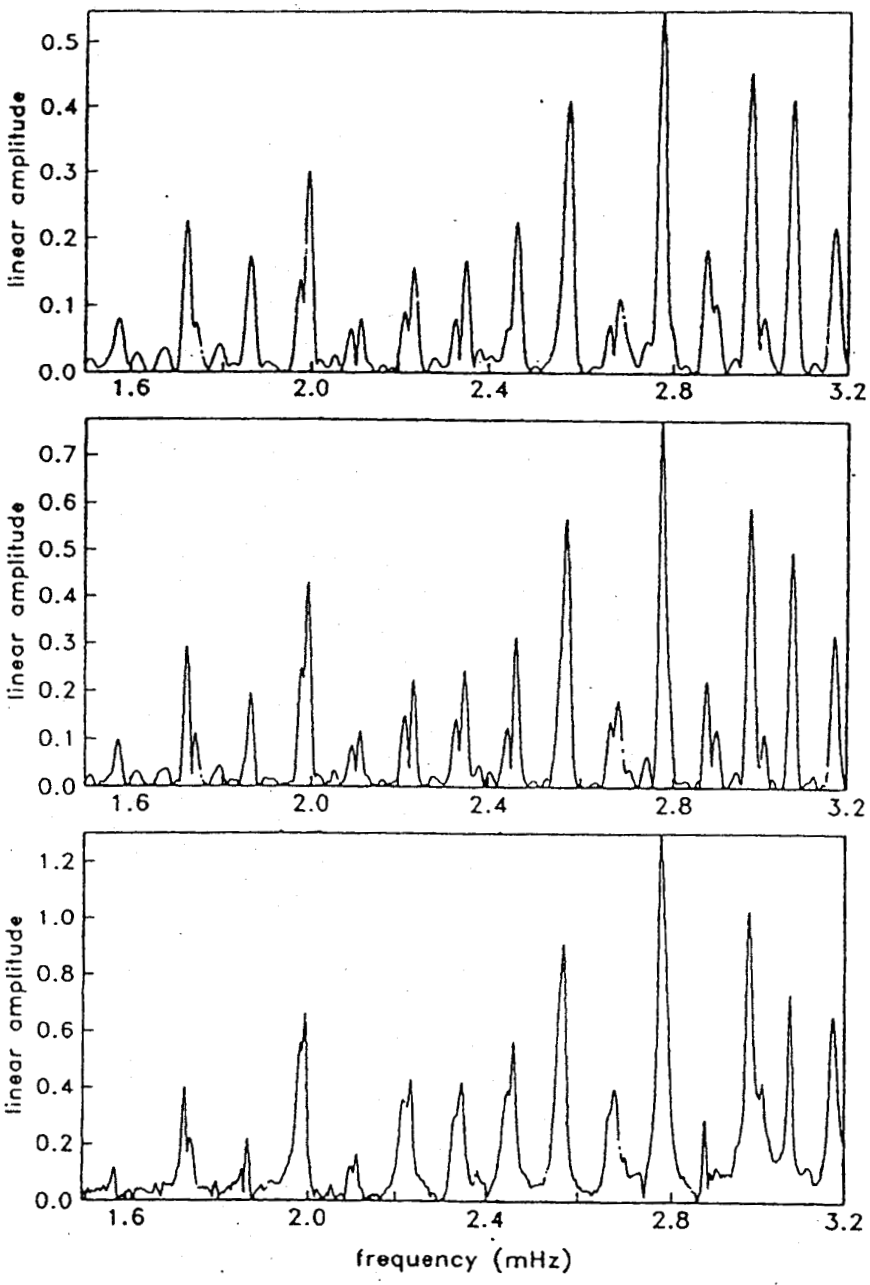

Figure 1.6. Direct spectral estimates of a 35-hour time series using a boxcar taper (lower panel), a 2π prolate taper (middle panel, and a 4π prolate (upper panel). In the lower panel, the distortion caused by spectral leakage is so great that the spectral estimate using a boxcar taper is useless. In the top panel, the peak widths are so broad that some multiplets are merged together. The middle panel gives a reasonable compromise between resolution and spectral leakage.

we obtain no estimate of the uncertainty in our estimate of ω_k. An obvious way to measure α_k is to use a "moving window" analysis. The amplitude of the spectrum of a segment of data is estimated and then the amplitude of a later segment of data is estimated. The drop in amplitude is related to α_k. Again, it turns out that this is not a good procedure and our resulting estimate of α_k is more uncertain than it need

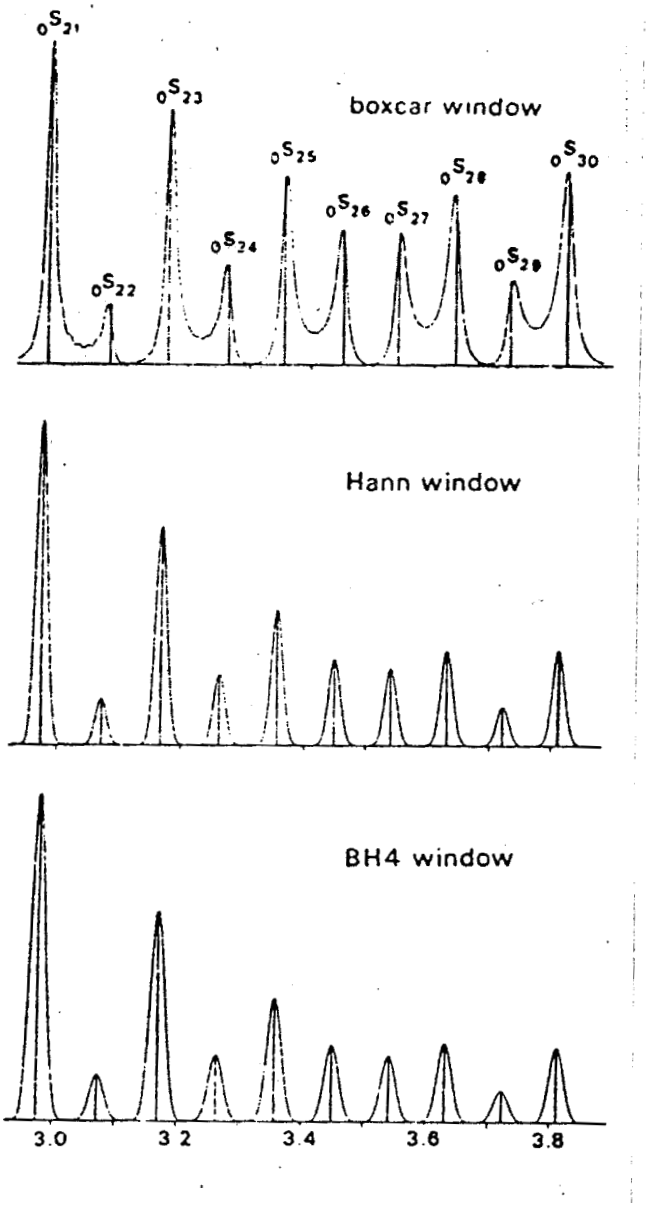

Figure 1.7. The effect of tapering on the spectra of synthetic seismograms which include fundamental modes only. In the top panel, note how peaks appear to be shifted away from their true frequencies

be.

An overview of measurement techniques can be found in Masters and Gilbert, (1983) and we briefly describe two of these here. For simplicity, we consider a single isolated mode of oscillation though it is desirable that any measurement technique can handle modes which overlap in frequency. We have

$$u(t) = A_k \cos(\omega_k t + \phi_k) e^{-\alpha_k t}$$

Fourier transforming gives

$$u(\omega) = a_k C_k(\omega) \tag{1.7}$$

where a_k is a complex number with

$$A_k = |a_k| \quad \text{and} \quad \phi_k = \tan^{-1}\left[\frac{Im(a_k)}{Re(a_k)}\right]$$

$C_k(\omega)$ is given approximately by 1.4.

You should note that a_k is linearly related to $u(\omega)$ in 1.7 whereas ω_k and α_k are nonlinearly related to $u(\omega)$. If ω_k and α_k are known it is therefore easy to recover a_k. In practice we work with a data window, $d(t)$ say, such as the Hanning taper and 1.7 becomes

$$u(\omega) * d(\omega) = a_k C_k(\omega) * d(\omega)$$

or

$$u'(\omega) = a_k C'_k(\omega) \tag{1.8}$$

We evaluate $u'(\omega)$ and $C'_k(\omega)$ at a small number of frequencies, ω_i, about the peak of interest, ***i.e.***,

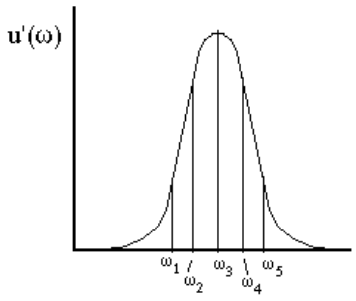

Let $u'_i = u'_i(\omega_i)$ and $C'_i = C'_k(\omega_i)$, then 1.8 can be rewritten in matrix form as

$$\begin{bmatrix} Re(u'_1) \\ Im(u'_1) \\ Re(u'_2) \\ Im(u'_2) \\ \vdots \end{bmatrix} = \begin{bmatrix} Re(C'_1) & -Im(C'_1) \\ Im(C'_1) & Re(C'_1) \\ Re(C'_2) & -Im(C'_2) \\ Im(C'_2) & Re(C'_2) \\ \vdots & \vdots \end{bmatrix} \begin{bmatrix} Re(a_k) \\ Im(a_k) \end{bmatrix} \tag{1.9}$$

Equation 1.9 is a set of simultaneous equations to be solved for a_k and may be solved by any of a number of techniques. We write 1.9 as

$$\mathbf{u'} = \mathbf{C'} \cdot \mathbf{a}$$

and the solution symbolically as

$$\mathbf{a} = \mathbf{C'^{-1}} \cdot \mathbf{u'}$$

(The least squares solution is $\mathbf{a} = (\mathbf{C'^T C'})^{-1}\mathbf{C'^T u'}$). Of course we need to know α_k and ω_k so that $\mathbf{C'}$ can be calculated but then $\mathbf{a}$ can easily be recovered. Equation 1.9 can also be easily modified if more than one mode is present in the spectrum.

If we do not know α_k and ω_k, we can make an initial guess and solve for a first estimate of a_k. Equation 1.8 can then be linearized so that a better estimate of ω_k and α_k can be found. We form

$$u'(\omega) = u'_0(\omega) + \frac{\partial u'_0(\omega)}{\partial \omega_k}\delta\omega_k + \frac{\partial u'_0(\omega)}{\partial \alpha_k}\delta\alpha_k \tag{1.10}$$

where $u_0(\omega)$ is formed using our initial estimates of ω_k, α_k and a_k. In the time domain it is easy to show that

$$\left.\begin{aligned} \frac{\partial u'_0(t)}{\partial \omega_k} &= -tA_k \sin(\omega_k t + \phi_k)e^{-\alpha_k t}d(t) \\ \frac{\partial u'_0(t)}{\partial \alpha_k} &= \ tA_k \cos(\omega_k t + \phi_k)e^{-\alpha_k t}d(t) \end{aligned}\right\} \tag{1.11}$$

Equation 1.11 can be easily Fourier transformed and 1.10 can then be cast into matrix form when all the terms dependent upon frequency are evaluated at a few frequency points about the peak of interest, *i.e.*, 1.10 becomes

$$\mathbf{u'} - \mathbf{u'_0} = \delta\mathbf{u'} = \mathbf{D}\cdot\mathbf{s} \tag{1.12}$$

where $\mathbf{s} = [\delta\omega_k, \delta\alpha_k]^T$ and $\mathbf{D}$ is a matrix of derivatives $\partial\mathbf{u'}/\partial\alpha_k$, $\partial\mathbf{u'}/\partial\omega_k$ evaluated at a few frequency points.

Solution of 1.12 follows the solution of 1.9. Once $\delta\omega_k$ and $\delta\alpha_k$ have been estimated, we form new estimates of ω_k and α_k (*i.e.*, $\omega_k \rightarrow \omega_k + \delta\omega_k$ and $\alpha_k \rightarrow \alpha_k + \delta\alpha_k$) and repeat the whole procedure until no improvement in fit to the data is obtained. Various tricks can be played to speed up convergence – see Masters and Gilbert (1983) for details.

An alternative technique (the autoregressive technique) which allows the estimation of ω_k and α_k in a noniterative fashion is based upon the recursion relations satisfied by a decaying cosinusoid. This method is described in detail by Chao and Gilbert (1980). Consider a single oscillation, *i.e.*, ,

$$u(t) = A_k \cos(\omega_k t + \phi_k)e^{-\alpha_k t} \tag{1.13}$$

Using trigonometric identies gives

$$u(t + \delta t) = y_1 u(t) + y_2 u(t - \delta t) \tag{1.14}$$

where δt is a time increment and

$$\left.\begin{aligned} y_1 &= 2\cos(\omega_k \delta t)e^{-\alpha_k \delta t} \\ y_2 &= -e^{-2\alpha_k \delta t} \end{aligned}\right\} \tag{1.15}$$

Suppose our time series is specified at evenly spaced time points, t_i, where $t_1 = 0, t_2 = \delta t, t_3 = 2\delta t$ *etc*. Then 1.14 can be written as

$$\begin{aligned} u(t_3) &= y_1 u(t_2) + y_2 u(t_1) \\ u(t_4) &= y_1 u(t_3) + y_2 u(t_2) \\ u(t_5) &= y_1 u(t_4) + y_2 u(t_3) \\ \vdots & \qquad\qquad \vdots \end{aligned} \tag{1.16}$$

which again can be cast in matrix form as

$$\begin{bmatrix} u(t_3) \\ u(t_4) \\ u(t_5) \\ \vdots \end{bmatrix} = \begin{bmatrix} u(t_2) & u(t_1) \\ u(t_3) & u(t_2) \\ u(t_4) & u(t_3) \\ \vdots & \vdots \end{bmatrix} \begin{bmatrix} y_1 \\ y_2 \end{bmatrix} \tag{1.17}$$

All the columns in 1.17 can be multiplied by a data window and Fourier transformed so that we need only use a few frequency points about a peak. Equation 1.17 can be solved for $\mathbf{y}$ then ω_k and α_k recovered from

$$\alpha_k = -\frac{1}{2\delta t} \ln(-y_2)$$
$$\omega_k = \frac{1}{\delta t} \cos^{-1}\left(\frac{y_1}{2\sqrt{-y_2}}\right).$$

This technique can be extended to handle more than one oscillation if our frequency band contains several modes. Both techniques described above have error analyses (Dahlen, 1982; Chao and Gilbert, 1980) so, in the presence of noise, we can assign uncertainties to our estimates of ω_k, α_k, A_k and ϕ_k. These error analyses also give an indication of the optimal record length to use for a particular data window. For a Hanning taper, a record length of 1.1 Q cycles is optimal for the recovery of α_k and ω_k.

A successful application of these techniques is shown in Figure 1.8. The dashed line is the original amplitude spectrum. The solid line is the residual after subtracting out a decaying sinusoid with the best estimates of A_k, ϕ_k, ω_k, and α_k. Figure 1.9 is an example of what happens when the spectrum does not correspond to that of a single decaying cosinusoid and the retrieved values of ω_k and α_k are unreliable. Another way of diagnosing failure of the techniques is to vary the record length used in the analysis. If the retrieved values of α_k and ω_k vary as the record length is changed, we are probably observing an interference effect and the spectrum again cannot be adequately modeled by a single decaying cosinusoid.

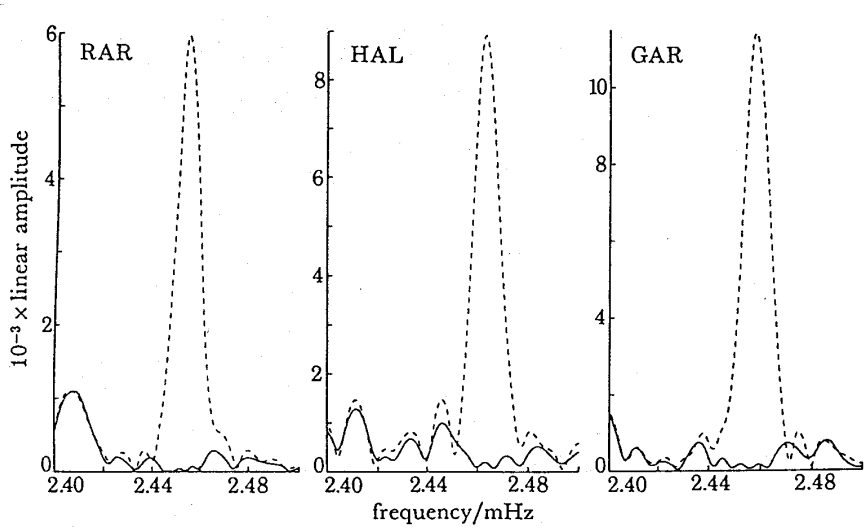

Figure 1.8. Three examples of successful demoding for the mode ${}_0S_{16}$. The original spectrum is shown by the dashed line and the residual spectrum is shown by the solid line.

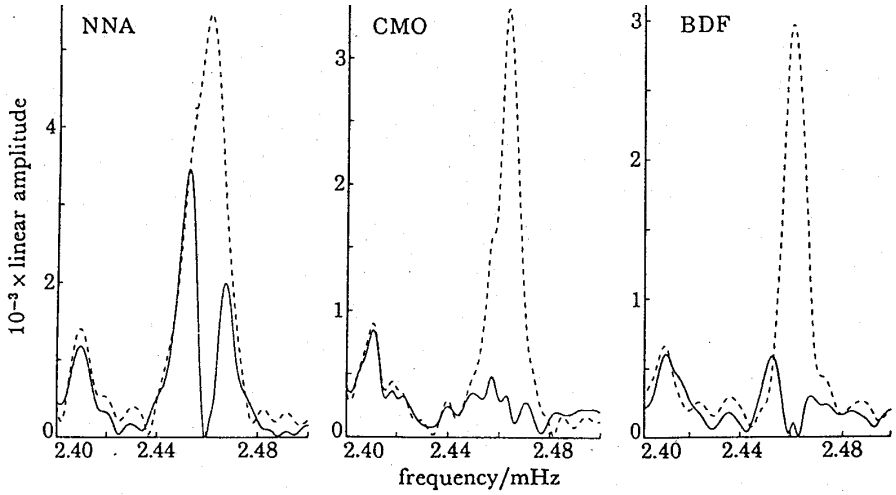

Figure 1.9. Three examples of unsuccessful demoding for the mode ${}_0S_{16}$. The large residual spectrum shows that the peaks are not singlet-like.

In successful cases, all techniques give the same answers as illustrated in Figure 1.10 (in the second panel we have plotted $1000/Q$ instead of α_k). Each point is an estimate made from a different seismic record of a mode of oscillation (in this case, ${}_0S_{13}$).

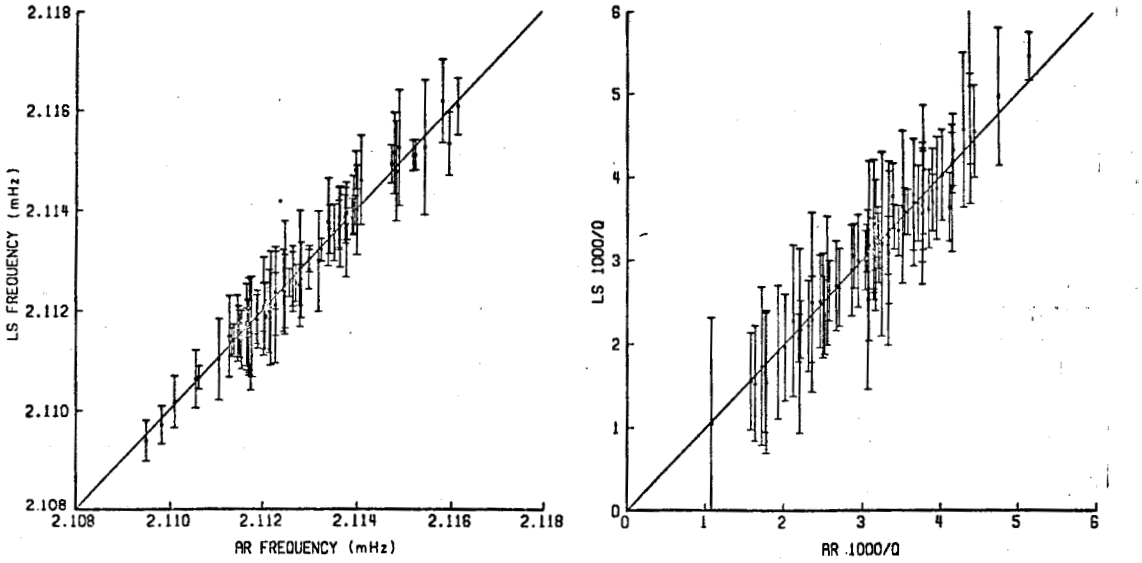

Figure 1.10. Comparisons of measurements of frequency (left side) between the AR and LS methods. The right side shows a comparison of $1000/Q$

If the Earth was truly spherically symmetric, ${}_0S_{13}$ would have the same frequency ($\sim$2.113 mHz) on every recording. The resolvable variation in measured frequency of this mode (2.1095 $\rightarrow$ 2.1162 mHz) is a consequence of the fact that the Earth is not quite spherically symmetric. Each seismic recording dominantly gives a sampling of the Earth which corresponds to the average structure under the great circle joining source and receiver. Thus each source-receiver pair samples a slightly different structure – faster paths give higher frequencies. In our example of ${}_0S_{13}$ there are 27 closely spaced modes of oscillation. The interference between the 27 oscillations results (usually) in a single peak which looks like a single resonance function. The peak frequency is variable (depending upon which great circle we are sampling) and the apparent attenuation that we measure is a mixture of true attenuation and beating effects.

At very long periods ($\sim$1000 seconds), the Earth's rotation is the dominant cause of splitting. The effect is so strong that we do not see a single peak anymore but a set of closely spaced peaks (Figure 1.11). The exception to this is at the South Pole where a vertical component recording should still show a single peak if rotation is the dominant cause of splitting. The lower panel in Figure 1.11 demonstrates this to be the case (look particularly at ${}_1S_4$). Unfortunately, at very low frequencies the South Pole is a noisy station so that no modes of oscillations are visible with frequencies less then $\sim$.4 mHz.

Splitting can lead to very strange estimates of apparent attenuation and it makes it very difficult to learn about the attenuative properties of the Earth.

As noted above, the techniques for measuring the properties of an oscillation of the Earth (A_k, ϕ_k, α_k, ω_k) can be easily extended to simultaneously measure the properties of several oscillations. An example of fitting two peaks is shown in Figure 1.12. Unfortunately, there are trade-offs between the parameters of the oscillations and it is difficult to obtain reliable estimates. There are two ways of avoiding multiple-peak estimation. One arises if the two modes have very different attenuation rates. If we choose a sample of data which starts late in the record, the strongly attenuated mode will have decayed much more than the weakly attenuated mode and, if we start late enough, we will effectively be left with a single mode. This is illustrated in Figure 1.13. The spectra are of 125 hours of recording but starting 2 hours, 27 hours, and 52 hours respectively after the origin time of the event. In the last panel we have almost removed the lower frequency, more highly attenuated mode. This is an example of the use of the Earth as an attenuation filter.

An alternative way of avoiding multi-peak estimation is to use many recordings and add them together in such a way as to emphasize a single mode of oscillation. We shall be developing the machinery required to perform this "array-processing" of data as the book progresses. For now, reconsider 1.8 when more than one mode is present, *i.e.*,

$$u'(\omega) = \sum_k a_k C'_k(\omega)$$

Now a_k is a function of the source-receiver geometry and the earthquake source mechanism, so for the jth recording we can write

$$u'_j(\omega) = \sum_k a_{kj} C'_k(\omega) \tag{1.18}$$

If a_{kj} can be computed, we can solve 1.18 for $C'_k(\omega)$, *i.e.*, the resonance function of individual modes of oscillation. Figure 1.14 shows a plot of $|C'_k(\omega)|$ in a small frequency band where a few modes of oscillation are present. About 800 recordings were used to solve for the $C'_k(\omega)$ and we have done a good job of isolating individual modes. We can now measure α_k and ω_k from the isolated resonance functions. With some assumptions, it is possible to compute a_{kj} for individual resonance functions within a nearly

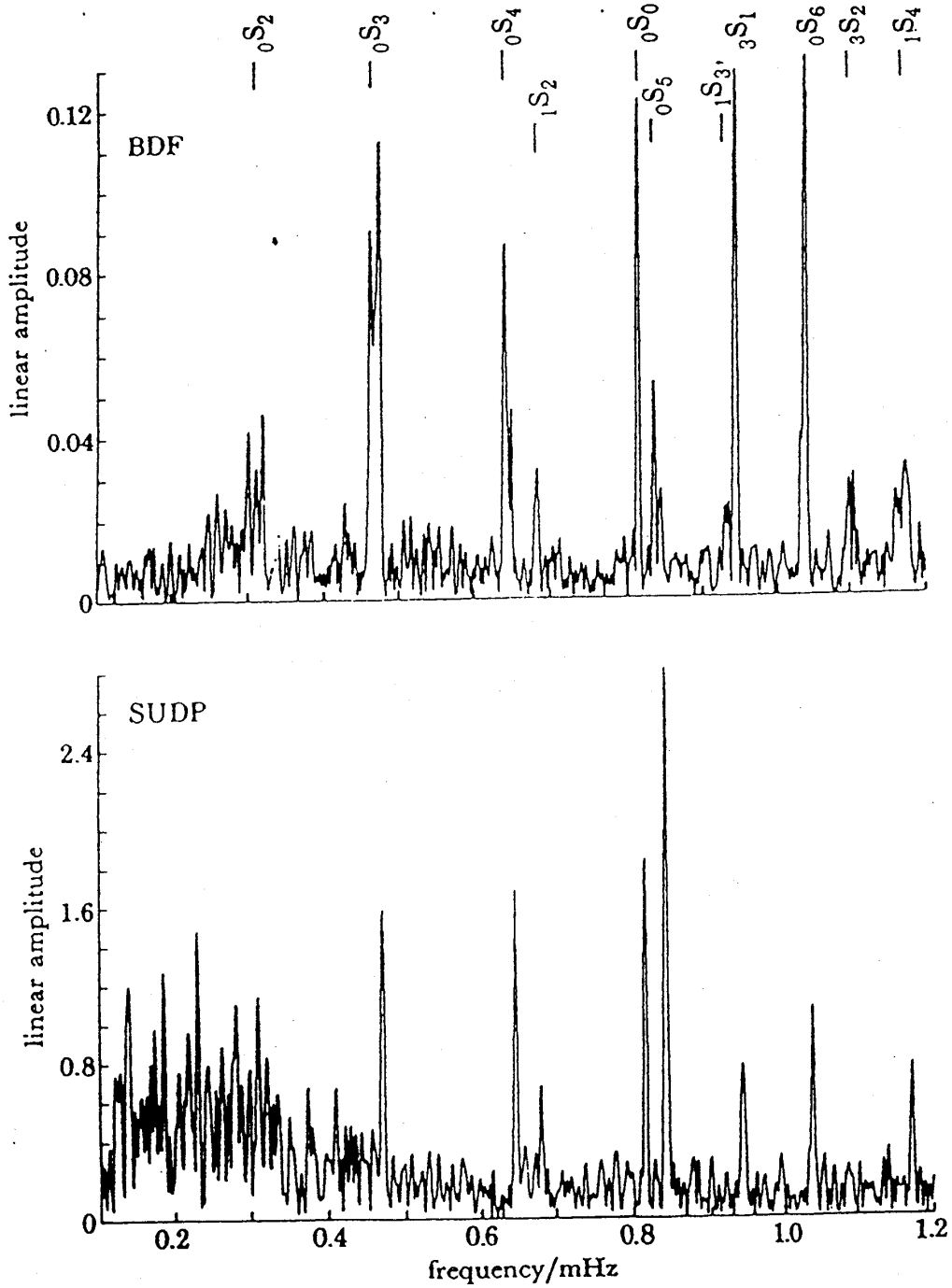

Figure 1.11. Two spectra of 120hr records from the Sumbawa earthquake of 1977. The effects of rotation and ellipticity cause obvious splitting at station BDF (Brasilia). The lower panel is a spectrum from a station at the South Pole which shows no sign of splitting (though it is noisy at frequencies below 0.4 mHz). The lack of splitting at the pole is expected if rotation and axisymmetric structure are the dominant perturbing influences.

degenerate multiplet. Figure 1.15 shows an application to the nine closely spaced singlets of $_1S_4$ again

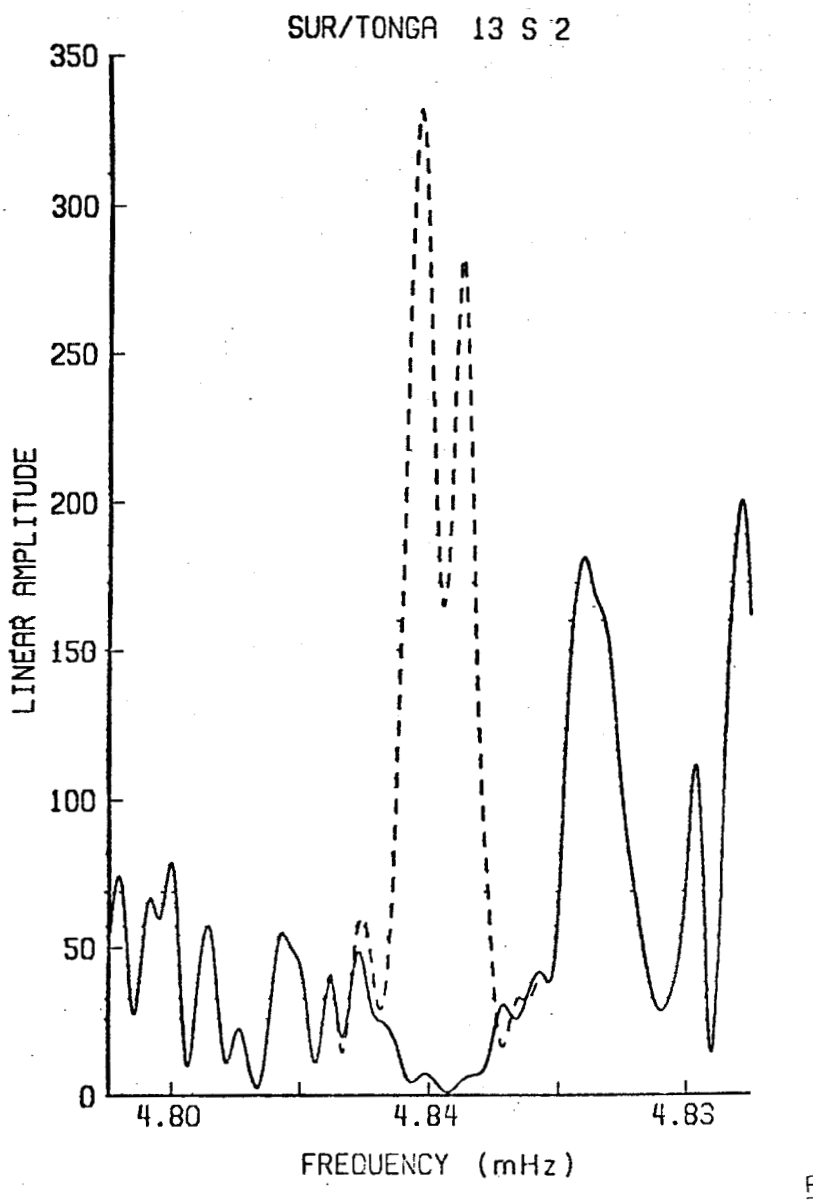

Figure 1.12. A simultaneous two-mode estimate for the strongly split multiplet ${}_{13}S_2$.

showing that fine-scale isolation of singlets is possible.

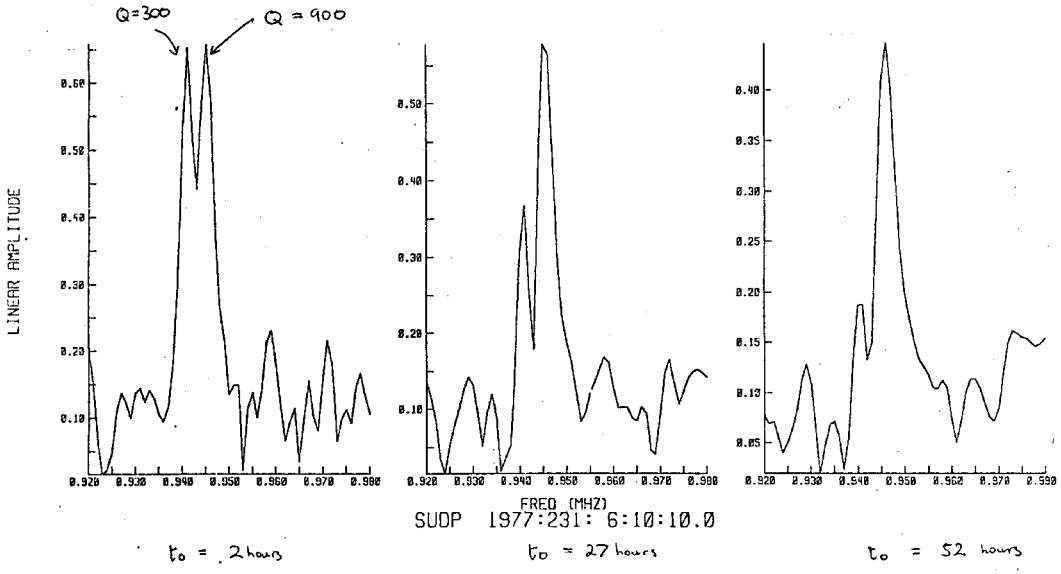

Figure 1.13. Using the Earth as an attenuation filter. Starting later in the record attenuates the lower Q mode more revealing the higher Q mode.

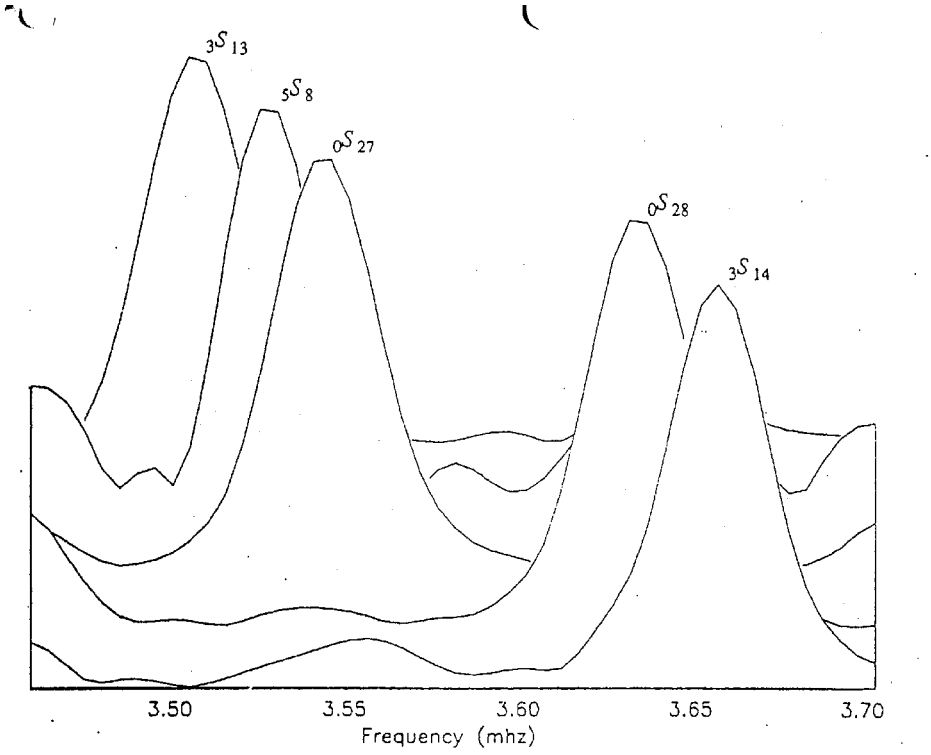

Figure 1.14. The result of stripping 800 recordings in a small frequency band which includes the fundamental modes ${}_0S_{27}$ and ${}_0S_{28}$. Each row of the figure is the amplitude spectrumof a single $C_k(\omega)$. Note that overtones are clearly separated from the fundamentals.

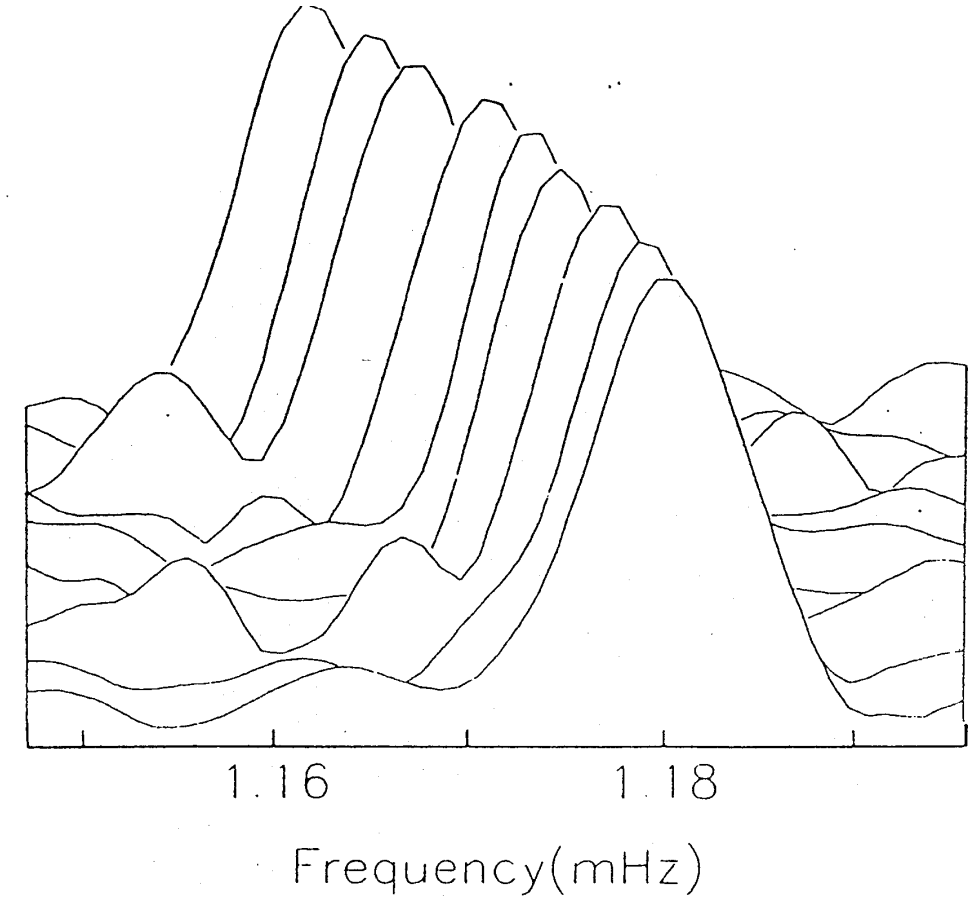

Figure 1.15. This figure has the same format as fig1.14 but now each row is the amplitude spectrum of a singlet of ${}_1S_4$. All nine singlets are recovered and follow a quadratic in azimuthal order close to that predicted for a rotating hydrostatic Earth.

1.3 References .

Chao, B.F., and F. Gilbert, Autoregressive estimation of complex eigenfrequencies in low frequency seismic spectra. *Geophys. J. R. Astron. Soc.*, **63**, 641–657, 1980.

Dahlen, F.A., The effect of data windows on the estimation of free oscillation parameters. *Geophys. J. R. Astron. Soc.*, **69**, 537–549, 1982.

Harris, F., On the use of windows for harmonic analysis with the discrete Fourier transform. *Proc. IEEE*, **66**, 51–83, 1978.

Masters, G., and F. Gilbert, Attenuation in the earth at low frequencies. *Phil. Trans. R. Soc. London*, **A308**, 479–522, 1983.

Thomson, D.J., Spectrum estimation and harmonic analysis. *IEEE Proc.*, **70**, 1055–1096, 1982.

1.4 Appendix: The general Prony's method .

This appendix gives the generalization of Prony's method to the case of several (complex) exponentials. Let

$$c_j = a_j e^{i\omega_j t_0} \quad \text{and} \quad v_j = e^{i\omega_j \delta t}$$

where t_0 is the start time if the time series and δt is the sample interval. Now suppose there are m exponentials in the time series $y_i, i = 0, ..., m$ where $y_0 = y(t_0), \quad y_1 = y(t_0 + \delta t), ...$ etc. Then

$$\begin{aligned} y_0 &= c_1 + c_2 + ... + c_m \\ y_1 &= c_1 v_1 + c_2 v_2 + ... + c_m v_m \\ y_2 &= c_1 v_1^2 + c_2 v_2^2 + ... + c_m v_m^2 \\ &\vdots \\ &\vdots \\ y_m &= c_1 v_1^m + c_2 v_2^m + ... + c_m v_m^m \end{aligned} \tag{1.19}$$

Now let $v = \exp(i\omega\delta t)$ and form the polynomial

$$(v - v_1)(v - v_2)\cdots(v - v_m) = s_0 v^m + s_1 v^{m-1} + \cdots + s_m = \Phi(v) \tag{1.20}$$

where, obviously, $s_0 = 1$ and the other s's are complicated functions of the v_i. Now multiply the first row of equation 19 by s_m, the second row by s_{m-1} and so on, then add all the rows together giving:

$$\begin{aligned} c_1(s_m + s_{m-1}v_1 + \cdots + s_0 v_1^m) + c_2(s_m + s_{m-1}v_2 + \cdots + s_0 v_2^m) \\ + \cdots + c_m(s_m + s_{m-1}v_m + \cdots + s_0 v_m^m) \\ = s_m y_0 + s_{m-1} y_1 + \cdots + s_0 y_m = c_1\Phi(v_1) + c_2\Phi(v_2) + \cdots + c_m\Phi(v_m) \end{aligned} \tag{1.21}$$

But when $v = v_i$, $\Phi(v_i) = 0$ and remembering that $s_0 = 1$ we get

$$s_m y_0 + s_{m-1} y_1 + \cdots + s_1 y_{m-1} = -y_m \tag{1.22}$$

which is our recursion relationship. The important thing is that equation 20 demonstrates that the coeficients in the recursion relation are also the coefficients in a polynomial whose roots are the v_i. We would now set up the matrix problem by taking m shifted versions of the time series as the matrix columns and a $m + 1$ shifted time series as the data column and solve equation 22 for the s's. By equation 20, the s's are the coefficients of a polynomial whose roots are v_n where

$$v_n = e^{i\omega_n \delta t}$$

so a root finding procedure (such as Bairstow's method) can be used to obtain the v_n once the s's are determined. The generalization to decaying cosinusoids (ie decaying modes) can be done in a straightforward fashion if we write the (real) time series as

$$y(t) = \sum_k \left[A_k e^{i\omega_k t} + A_k^* e^{-\omega_k^* t} \right]$$

where A and ω are now both complex. The reader is referred to Chao and Gilbert (1980) for details.